Towards Proton Therapy and Radiography at FAIR

M. Prall[1], P. M. Lang[1,2], C. LaTessa[1] F. Mariam[3] , F. Merrill[3], L. Shestov[1], P. Simoniello[1], D. Varentsov[1] and M. Durante[1]

[1]GSI Helmholtzzentrum für Schwerionenforschung GmbH, Planckstraße 1, 64291 Darmstadt, Germany
[2]TU Darmstadt, Schlossgartenstraße 9, 64289 Darmstadt, Germany
[3]Los Alamos National Laboratory, Los Alamos, NM 87545, USA

E-mail: m.prall@gsi.de

Abstract. Protons having energies in the GeV range have been proposed as an alternative to Bragg-peak hadron therapy. This strategy reduces lateral scattering and overcomes uncertainties of particle range and relative biological effectiveness. GeV protons could additionally be used for targeting in image guided stereotactic radiosurgery. We experimentally demonstrated the potential of GeV protons for imaging of biological samples using E=0.8 GeV protons and the pRad setup at Los Alamos National Laboratory (LANL). In this setup, a system of magnetic lenses creates a point-to-point mapping from object to detector. This mapping compensates image blur due to lateral scattering inside the imaged (biological) object. We produced 2-dim proton radiographs of biological samples, an anthropomorphic phantom and performed simple dosimetry. High resolution tomographic reconstructions were derived from the 2-dim proton radiographs. Our experiment was performed within the framework of the PANTERA (Proton Therapy and Radiography) project. In the future, the proton microscope PRIOR (Proton Microscope for FAIR) located in the FAIR facility (Darmstadt), will focus on optimizing the technique for imaging of lesions implanted in animals and couple the irradiation with standard radiotherapy.

1. Introduction

Proton therapy plays an important role in the treatment of cancer [1] and noncancer [2] diseases. More than 50% of patients with localized malignant tumors are nowadays treated with radiation [3]. The challenge in radiotherapy is to deliver ionizing irradiation such that the target region is ablated or sterilized, whereas the surrounding healthy tissue is spared. Protons having energies between about 60 and 250 MeV are well suited for this purpose due to their depth-dose profile (Bragg curve). The proton beam has a finite range in matter and deposits most of its energy at the end of its path (cf. Figure 1).

In treatment of cancer, typically several 10.000 Bragg-peaks are placed in a tumor volume. The depth (range) of each Bragg-Peak is adjusted via its initial energy. The lateral beam position can be adjusted by dipole magnets in the beam line. This so-called rasterscan technique was used to treat more than 450 patients in a pilot experiment at GSI [3] and is now implemented e.g. at Heidelberg Ion Beam Therapy Centre (HIT), where up to 1000 patients are treated each year. Yet, in Bragg-peak therapy the beam profile is broadened by multiple scattering in the patient's tissue. This produces a dose-halo around the target, which is typically a few mm wide. This can be problematic if life-critical structures e.g. in the brain are close (a few

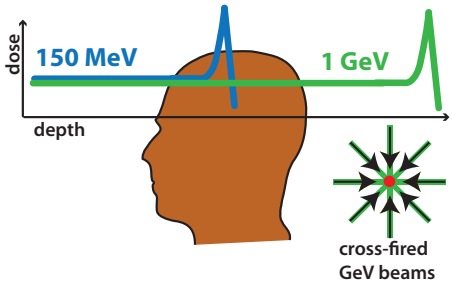

Figure 1. Comparison of Bragg peak therapy and GeV particle radiosurgery. The two graphs (150 MeV and 1 GeV) symbolize the depth-dose profiles in Bragg-peak and GeV therapy. Whereas the dose-maximum is placed inside the target in Bragg-peak therapy (here: the head), GeV beams have to be cross-fired to achieve a dose-maximum at their intersection (see bottom right).

mm or less). Lateral scattering of a proton is roughly proportional to $1/\beta^2$, where $\beta = v/c$ [4]. Therefore, lateral scattering can be significantly reduced by increasing the particle velocity β. Using protons having energies of about a GeV reduces lateral scattering to the sub-mm region [5]. However, a target cannot be treated from a single direction any more. Several GeV beams have to be cross-fired from different angles. This situation is sketched in the insert of Figure 1.

Clinical experience with cross-fired GeV proton beams has already been gained since 1975 at PNPI St. Petersburg with about 1300 patients [8]. Targets in the brain, e.g. cerebral artery-venous malformations, pituitary adenomas, but also outside the brain, like prostate cancer were treated successfully. Patients were aligned using X-rays.

Although GeV protons are used in the plateau region (cf. Figure 1), the depth-dose distribution is not flat [5]. Knock-out and evaporation hadrons, mostly secondary protons from nuclear interactions cause an increase of the overall dose deposition. These effects have already been studied for shielding of relativistic protons for space radiation protection [9]. Whereas the contribution of primary protons decreases by a few percent, the overall dose increases by $30 - 40$ % after about 20 cm of tissue [5]. These effects will be studied in more detail in order to include them into treatment planing for IGSpRS (Image Guided Stereotactic proton Radiosurgery). In IGSpRS, the beam, which has passed the patient is used for simultaneous radiography (imaging) of the treated region.

2. Image guided stereotactic radiosurgery with a proton microscope

Whereas a drawback of GeV radio surgery is the loss of the Bragg-peak, a valuable advantage is that IGSpRS becomes possible. IGSpRS allows to detect misalignments of the patient or a change of the target region online. This is not possible with the combination of computerized X-ray tomography, 2-dim X-ray imaging and immobilization devices used today in clinical practice. IGSpRS would be advantageous for patients with the above-mentioned diseases, especially close to life-critical structures.

The spatial resolution of conventional proton radiography based on energy loss is limited and thus its practical applicability [6]. A proton microscope (PM) compensates image blur using magnetic lenses to the sub-mm level. We are therefore aiming to realize IGSpRS with a PM at FAIR. Ignoring effects such an energy loss in the imaged object, a PM (cf. Figure 2) works as follows: After crossing a part of the patient with thickness d and radiation length L_{rad}, protons exit tissue with angles θ with respect to the initial beam axis z. The trajectory through the PM depends on the exit angle θ. A first set of magnetic lenses (A) transforms the angle θ into a distance from the beam axis at the position of the collimator (B). The larger θ, the larger the distance from the beam axis z. The collimator (B) suppresses protons having more than a certain distance from the beam axis and thus a scattering angle larger than a critical scattering angle θ_c. A second set of magnetic lenses (C) after the collimator reverses the effect of the lenses before the collimator (A) such that one obtains a point-to-point mapping between the exit coordinates at the patient (x_0, y_0) and at the detector (x_1, y_1). Magnetic fields can

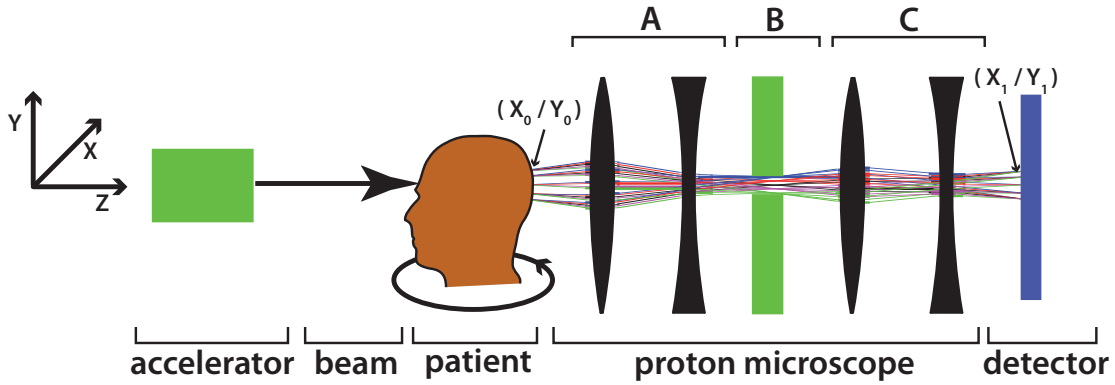

Figure 2. Image guided stereotactic proton radiosurgery using a proton microscope. The patient is rotated and beams are cross-fired through the target (e.g. a tumor). A proton microscope is used for simultaneous sub-mm resolution radiography of the treated region.

be chosen such that the image on the detector is larger than the radiographed object itself. Therefore the name proton *microscope*. In our case, fields were chosen such that a 1:1 mapping (without magnification) was achieved. The distribution of the exit angles θ can be described by a Gaussian having a standard deviation of $\sigma(\text{rad}) = \frac{14.1\ MeV}{\beta p}\sqrt{d/L_{rad}}$, where $\beta = v/c$ and $p =$ proton momentum. The larger the path length d through tissue, the more protons leave the patients with larger angles θ, the more are suppressed by the collimator and the fewer reach the detector. Additionally, nuclear interactions lead to particle loss equal to $\exp(-d/\lambda)$, where λ is the nuclear interaction length. Putting together nuclear losses and suppression of scattering angles $\theta(d)$ above a critical angle θ_c by the collimator leads to a transmission probability $T(d)$:

$$T(d) = \exp(-d/\lambda) \cdot \left(1 - \exp\left(-\frac{1}{2}\frac{\theta_c \beta p}{14.1\ \text{MeV}}\frac{L_{rad}}{d}\right)\right) \tag{1}$$

The count rate on each point of the detector is proportional to $T(d)$. However, this formula cannot be inverted analytically to determine d from a count rate. In practice one uses careful calibration measurements instead. These also include the influence of any other material (e.g. beam windows) in the beam line, as well as the initial angular spread of the beam. At LANL, the detector is a scintillator screen (SC). Once a proton pulse, having a width comparable to the size of this screen crosses the patient, the instrument and eventually the SC, a camera makes a black and white image of the SC light output. This image shows the path length through the patient d with sub-mm resolution. Via (1) the grey values in this image correspond to the path length d through the patient.

In the above description, we ignored effects leading to image distortion and finite spatial resolution. In reality, lateral drift of protons inside the imaged object, energy inhomogeneity coming from both, the initial beam and inhomogeneous energy loss inside the imaged object, off-axis effects, the choice of the SC and the light optics through which the SC is filmed, determine the spatial resolution of the data. For our biological samples and an E=800 MeV beam, the overall resolution is in the order of tenths of millimeters. A thorough review of charged particle radiography is given in [10].

3. Proton radiography and tomography of biological samples

In order to experimentally demonstrate the potential of a PM for biomedical applications, we made measurements with the PM of the pRad facility of LANL which uses an 800 MeV proton

beam [7]. The field of view of this instrument is about 10 cm x 10 cm. We produced 2-dim proton radiographs of biological samples, an anthropomorphic phantom and performed simple dosimetry. High resolution tomographic reconstructions using filtered backprojection [11] were derived from the 2-dim proton radiographs. Figure 3 gives an overview over our results, which will be presented more thoroughly in a forthcoming publication.

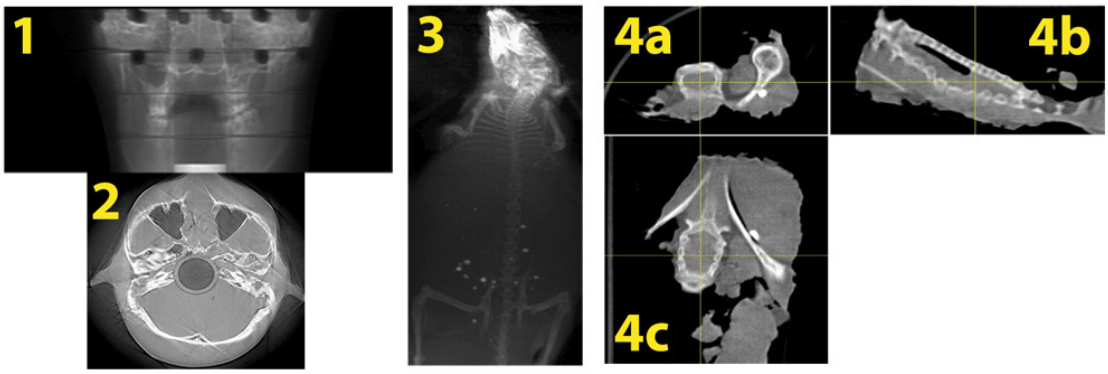

Figure 3. Some results: 1) Radiograph of a head phantom, 2) tomographic slice of a head phantom, 3) maximum intensity projection derived from a tomograph of a mouse, 4a) tomographic slice of a chicken sample, 4b) and 4c) orthogonal views of 4a).

4. Discussion

Measurements with thermoluminescent dosimeters inside the skull of the anthropomorphic phantom were made. These show that bony anatomy is clearly resolved with a dose of about $D_{image} \approx 10$ mGy. These structures could be used for position verification in IGSpRS. We expect that further measurements would allow to determine an even smaller value for D_{image}. At LANL, we use only two sets of thermoluminescent dosimeter (TLDs) for two independent dose measurements. For measurements, the TLDs were placed in slits inside the phantom and were later read out at DLR (Deutsches Zentrum fr Luft und Raumfahrt, German Aerospace Center) in Germany. This dose of $D_{image} = 10$ mGy is already negligible compared to target doses of up to 150 Gy used in proton radiosurgery [8]. The spatial resolution of the 2-dim proton radiographs is about 0.2 mm at high contrasts. 3-dim tomographic reconstructions derived from 2-dim radiographs show finest bony structures like ribs of the embedded mouse, substructure is visible in muscle-tissue of chicken samples, implanted steel and aluminum markers (not shown in Figure 3) are clearly resolved and do not produce artifacts in the 3-dim reconstructions. The world's first proton tomographic image of a skull was derived from our raw data. X-ray CTs of most samples were made using a state-of-the-art CT scanner (Biograph TruePoint by Siemens Healthcare, Forchheim, Germany). Reconstruction artifacts (streaks and ring artifacts) are visible in the proton tomographs. Yet the tomographic slices are comparable to the X-ray CTs (not shown). Artifact suppression is algorithmically challenging, a subject of current research [12] and beyond the scope of our study.

Recent studies on ion CT employ either complex or expensive detector designs [13, 14, 15, 16] or a time-consuming data acquisition strategy using a scanned beam [17]. In our method, the time for a proton CT is limited by the speed of the rotary table on which the imaged sample is placed and could be reduced to a few seconds for a tomographic scan. In the future, this feature might be important for clinical applications, where a proton CT scan should not take longer than a few seconds.

5. Outlook

Our study has clearly demonstrated the potential of a PM for IGSpRS and imaging in 2 and 3 dimensions. The encouraging clinical results obtained at PNPI with 1 GeV protons [8], support the rationale for IGSpRS for future clinical applications in radiosurgery at FAIR. Especially a subgroup of patients having life-threatening cancer- and noncancer diseases close (a few mm or less) to life-critical structures will benefit significantly from this bloodless treatment modality.

Within the PaNTERA (Proton Therapy and Radiography) project, we are mostly interested in imaging biological samples. Tomography is, of course not limited to these. Actually in many applications is becomes superior to x-ray CT, when the object is too dense or too thick for X-rays. At LANL, for example one has already studied damage detection in nuclear fuel pellets with this method [10]. A feature of a PM, that we did not use is the ability to produce short series of radiographs having microsecond spacing [10]. This allows to study dynamic processes like explosions or impacts in 2 dimensions.

At FAIR, the proton microscope PRIOR will not only be used for IGSpRS. A wide range of interdisciplinary experiments will be performed. These are e.g. experiments on fundamental properties of materials in extreme dynamic environments generated by external drivers (pulsed power drivers, high energy lasers, gas guns or HE generators) prominent for materials research and non-ideal plasma physics.

6. Acknowledgements

We thank Dr. Julia Bauer (HIT Heidelberg) for performing x-ray CT scans of our samples. Dr. Thomas Berger (DLR) and his team provided the human phantom and radiation detectors. They also took care of the detector readout. Last but not least, we thank the staff of pRAD for experimental support and fruitful discussions.

References

[1] M Durante and J Loeffler Nat. Rev. Clin. Oncol. 7 37
[2] C Bert, R Engenhart-Cabillic and M Durante Med. Phys. 39 1716
[3] Schardt D, Elsässer T, Schulz-Ertner D. Rev Mod Phys 2010;82:383
[4] H Paganetti Proton Therapy Physics, CRC Press, ISBN: 978-1-4398-3644-6
[5] M Durante and H. Stöcker Journal of Physics: Conference Series 373 (2012) 012016
[6] J M Schipper and A J Lomax 2011 Acta Oncol. 50 838
[7] N S P King, E Ables, K Adams, et al. NIMA, 1999, 424: 84-91.
[8] N K Abrosimov et al. Journal of Physics: Conference Series 41 (2006) 424-432
[9] M Durante and F A Cucinotta 2011 Rev. Mod. Phys. 83 1245
[10] C L Morris et al. Rep. Prog. Phys. 76 (2013) 046301 (26pp)
[11] A C Kak and M Slaney Principles of Computerized Tomographic Imaging (1988)
[12] T M Buzug, Computed Tomography From Photon Statistics to Moden Cone-Beam CT, Springer, ISBN: 978-3-540-39407-5
[13] Sadrozinski H-W et al 2003 Nucl. Instrum. Methods Phys. Res. A 511 27581
[14] Ohno Y, Kohno T, Matsufuji N and Kanai T 2004 Nucl. Instrum. Methods Phys. Res. A 525 27983
[15] Murashi H et al 2007 IEEE Nucl. Sci. Symp. Conf. Record pp 43548
[16] U Amaldi et al. Nucl. Instrum. Methods Phys. Res. A 629 33744
[17] J Telsemeyer, O Jaeckel and Maria Martisikova Phys. Med. Biol. 57 (2012) 79577971